Activation of Dioxygen by a TAML Activator in Reverse Micelles:

Characterization of an $Fe^{III}Fe^{IV}$ Dimer and Associated Catalytic Chemistry

Liang L. Tang, William A. Gunderson, Andrew C. Weitz, Michael P. Hendrich,* Alexander D. Ryabov* and Terrence J. Collins*

Department of Chemistry, Carnegie Mellon University, 4400 Fifth Avenue, Pittsburgh, Pennsylvania 15213, United States

---

Supporting Information

Experimental Details

Methods

NADH and NAD^+ analysis by HPLC. The 250×4.6 mm Agilent Microsorb-MV 100 C18 column was used for NADH and NAD^+ analysis.

Method 1. Two eluents were employed which is a simplified method of method 2. Eluent A was a 0.05 M potassium phosphate buffer, pH 6.0; eluent B was a mixture v/v of 60% A and 40% MeOH. The temperature was maintained at 40 °C across the column. The gradients used as described elsewhere[1] are shown in Table S1. The flow rate was constant 1.0 mL/min.

Method 2. The HPLC utilized four eluents. Eluent A was a 0.05 M potassium phosphate buffer, pH 6.0; eluent B was a mixture v/v of 60% A and 40% MeOH; eluent C was 100% MeOH; eluent D was HPLC grade water. The temperature was maintained at 40 ℃ across the column. The gradient used is shown in Table S2.[1] The flow rate was constant 1.0 mL/min.

The extraction of products from the reverse micelles was initiated by addition of 2 mL water to 2 mL reaction mixtures. After vigorous shaking, the emulsion was centrifuged at 8000 rpm for 10

min using an Eppendorf minispin centrifuge. The aqueous bottom phase was removed by a glass pipet and analyzed.

Procedures

For the reaction of **2a** with NADH in the absence of oxygen, the "freeze-pump-thaw" method was applied. A mixture of unpurified AOT in *n*-octane (19.75 mL, 0.1 M), NADH in water (100 μL, 0.04 M) and pH 12 buffer (150 μL, w_0 7) in a 50 mL Schlenk flask was degassed three times (solution A). Solution A (1.5 mL) was added to a capped quartz cuvette containing 1.5 mL methanol and shaken fiercely. Two transparent layers formed after standing and the UV-vis spectrum of the lower layer (methanol) was measured. The methanol layer was further used for HPLC measurement (1 mL water was added to 1 mL methanol solution to prepare the HPLC sample). Compound **2a** (6.37 mg, 4×10^{-6} mol) in a 5 mL two-necked round bottom flask was degassed and degassed acetonitrile (500 μL) was added. The solution of **2a** (231 μL) was added to solution A and stirred for 20 min. The color of the mixture turned from light brown to light yellow and 1.5 mL was added to methanol (1.5 mL) for UV-vis measurements. Methanol was used because **2a** turns back to **1a** within 1 min in this solvent.[2] For the experiment with **1a**, similar procedure was used. Unpurified AOT in *n*-octane (9.875 mL 0.1 M), NADH in water (50 μL 0.04 M), pH 12 buffer (25 μL) and acetonitrile (125 μL) in a 25 mL Schlenk flask were degassed three times (solution B). Compound **1a** (9.3 mg, 2×10^{-5} mol) dissolved in pH 12 buffer (500 μL) was degassed. Compound **1a** (50 μL) was then added to solution B (w_0 7). Table S3 shows the results of the experiments obtained by HPLC method 2.

Table S1. HPLC Method 1 eluent gradient for the analysis of NADH and NAD^+.

Time (min)*	% Eluent A**	% Eluent B***
0.0	100	0
4.0	100	0
5.0	98.5	1.5
10.0	96.5	3.5
15.0	96.5	3.5
15.1	75	25
30.0	75	25
32.0	100	0
35.0	100	0

*The flow rate was constant 1.0 mL/min.

**Eluent A is 0.05 M phosphate buffer, pH 6.0.

***Eluent B is 60:40 v/v A: MeOH.

Table S2. HPLC Method 2 eluent gradient for the analysis of NADH and NAD^+.

Time (min)*	% Eluent A**	% Eluent B***	% Eluent C****	% Water
0.0	100	0	0	0
9.0	100	0	0	0
10.0	98.5	1.5	0	0
15.0	96.5	3.5	0	0
20.0	96.5	3.5	0	0
20.1	75	25	0	0
28.0	75	25	0	0
29.0	0	0	100	0
40.0	0	0	100	0
45.0	0	0	0	100
50.0	100	0	0	0
55.0	100	0	0	0

*The flow rate was constant 1.0 mL/min.

**Eluent A is 0.05 M phosphate buffer, pH 6.0.

***Eluent B is 60:40 v/v A: MeOH.

****Eluent C is 100% MeOH.

Table S3. Results of HPLC study of reactions of NADH (2.1×10^{-4} M) with iron(III) (**1a**) and iron(IV) (**2a**) species (both 2.0×10^{-4} M with respect to a monomeric form) in the reverse micelles at w_0 7 and pH 12.

Iron Species	Amount with respected to added NADH / %		Yield of NAD^+ with respect to total iron / %	Conditions
	NAD^+	NADH		
None	0	100	0	Solution A
2a	25	70	52	Reaction time 20 min
2a	85	0	180	After exposure to air for 15 min following the reaction
1a	7	82	14	Reaction time 20 min
1a	63	1	132	After exposure to air for 15 min following the reaction

Table S4. Comparison of the efficacy of catalysis by **1a** in oxidation of Pinacyanol chloride (PNC) (4.5×10^{-5} M) by O_2 in reverse micelles under different conditions at 25 °C.

w_0	$10^7\times$[**1a**]/M	Time/h	PNC bleached as measured at 600 nm / %		
			pH 8	pH 10	pH 12
			With/without **1a**		
3	5	48	44/11	43/11	67/8
	12.5	16	51/5	46/5	64/4
	50	3	24/0.2	8/0.3	22/0.1
10	5	16	62/5	84/9	100/5
	12.5	3	37/1	66/1	95/1
	50	3	96/1	97/1	97/1
25	5	48	42/10	82*/24	100*/6
	12.5	16	13/3	40/4	99*/2
	50	3	22/2	43/1	39/1

* A gradual change of color was observed in the cuvette and a darker color was at the bottom (no precipitate observed) which is supposed to be attributed to the instability of the reverse micelle system.

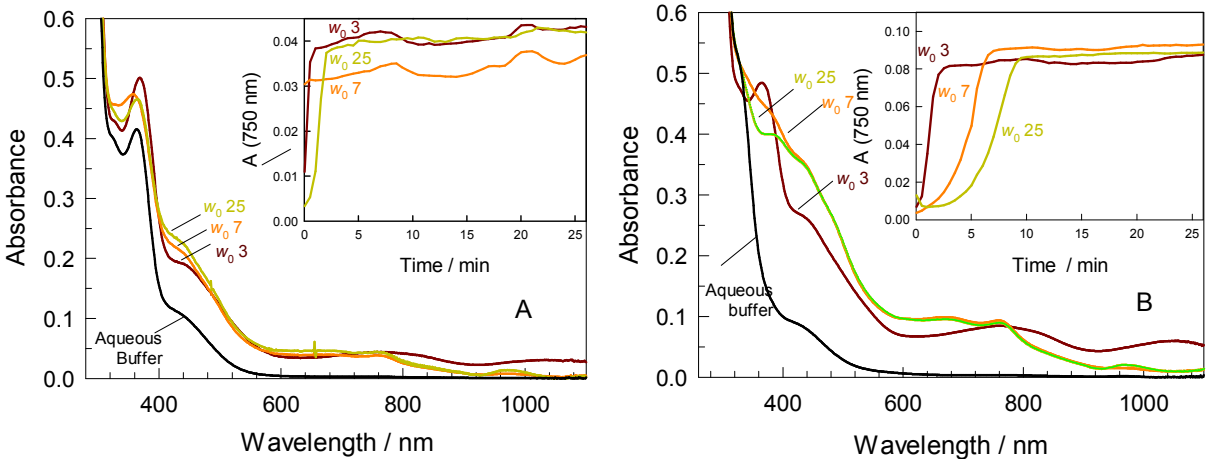

Figure S1. Spectra of **1a** in the AOT reverse micelles in *n*-octane recorded 20 min after mixing all components. The spectrum of **1a** in the aqueous buffer (bottom) is shown for comparison. Conditions: [**1a**] 1.36×10^{-4} M, pH 10 (**A**) and 12 (**B**), w_0 = 3, 7 and 25; 25 °C. Inset shows changes of absorbance at 750 nm with time at different w_0.

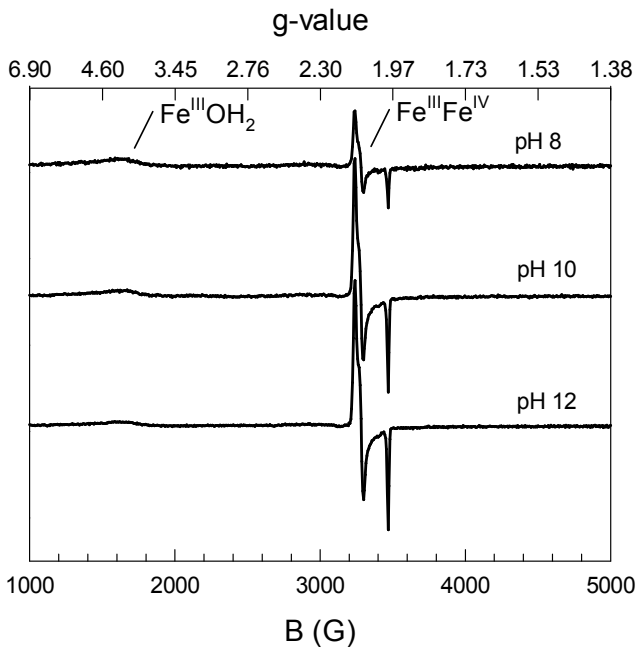

Figure S2. EPR spectra of **1a** in reverse micelles, w_0 10 at different pHs. Total iron 1.53×10^{-4} M. Measured concentrations of $Fe^{III}Fe^{IV}$ as dimer are 1.0×10^{-5} M, 2.5×10^{-5} M and 2.8×10^{-5} M at pH 8, 10 and 12, respectively.

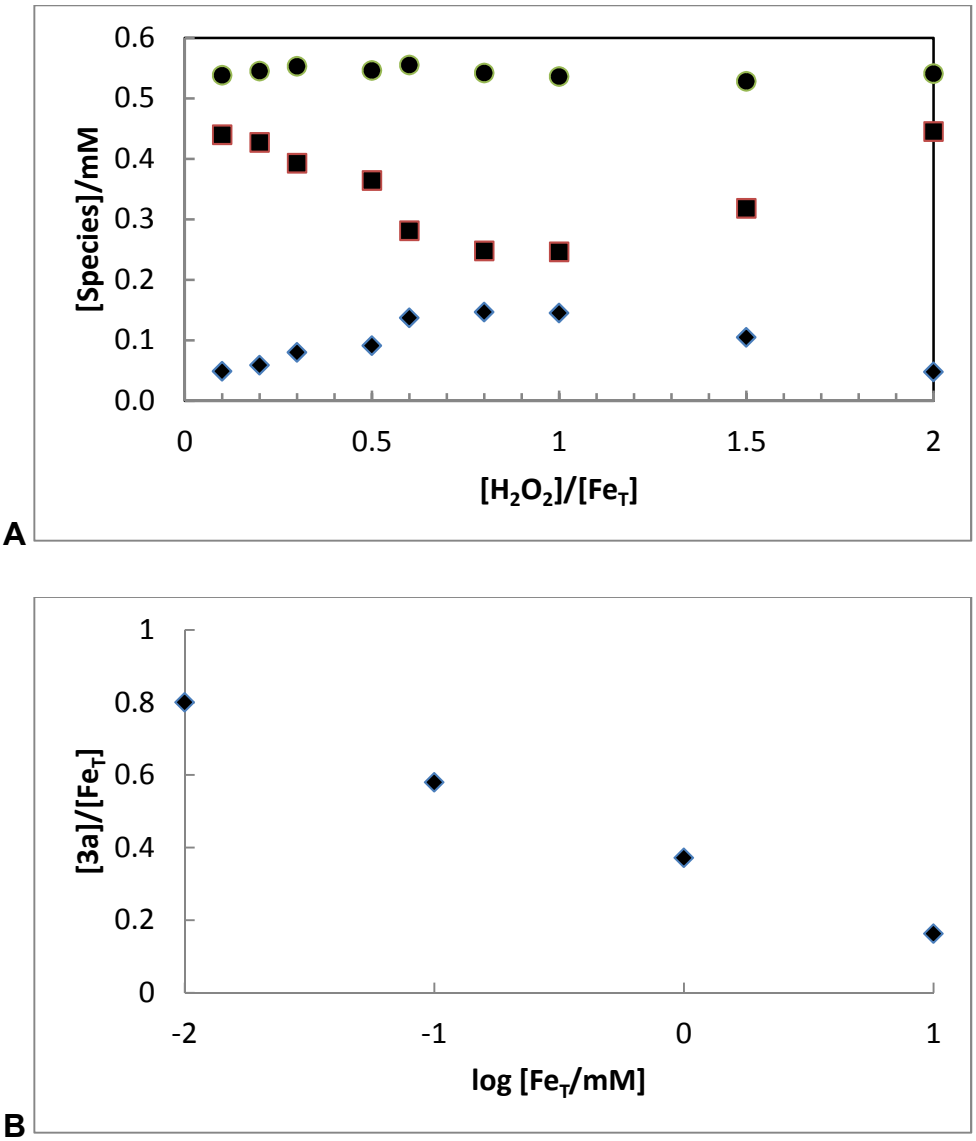

Figure S3. (**A**) Species concentrations of **1a** (■), **3a** (♦), and total Fe associated with both species (●) observed in EPR samples as a function of H_2O_2 added to 1 mM **1a**. (**B**) Concentration of **3a** after addition of 1 eq H_2O_2 to **1a** as a function of total Fe in the sample. All samples prepared in 50% glycerol, pH 11.8 (0.01 M phosphate) at –20 ºC.

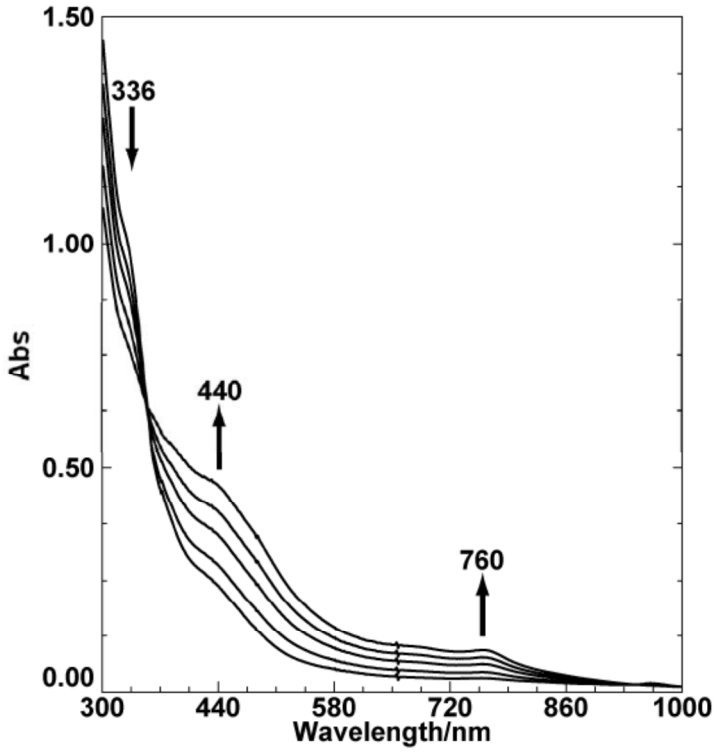

Figure S4. Absorption spectra of **3a** as formed from **1a** + H_2O_2. The spectra are shown for additions of 0.2, 0.4, 0.6 and 0.8 eqs of H_2O_2. The absorption bands at 440 and 760 nm grow with each addition, while the band from **1a** at 336 nm decreases in intensity.

Determination of Exchange Coupling

The EPR spectrum of **3a** was recorded at temperatures between 2 and 46 K. At each temperature the spectrum was recorded with a series of powers from 2 μW to 455 mW. The peak-to-peak signal intensity of the resonance at g = 2.111 as a function of microwave power was fitted to Eq. S1 to determine the power at half saturation, $P_{½}$, where D is the value of signal/$P_{½}$ for non-saturating (low) powers.

$$S/\sqrt{P} = D/(1 + P/P_{½})^{½} \quad \text{(S1)}$$

$$P_{½} = AT + BT^{n} + C[\exp(\Delta/T) - 1]^{-1} \quad \text{(S2)}$$

A plot of $P_{½}$ vs. T is shown in Fig. S5. Under the assumption that $P_{½}$ is proportional to the spin-lattice relaxation time, the power saturation contains terms for three relaxation processes: Direct, Raman and Orbach, respectively, which are fit with eq S2.[3] The energy of the first excited doublet relative to the ground doublet is Δ, and for Kramers systems n = 9. The constants A, B, C, and Δ are determine by least-squares fit to the data of Fig. S5. A fit to the data is shown in Fig. S5 for Δ = 90±30 cm^{-1} with additional fitting parameters given in the figure caption. The dashed line is a least-squares fit to the data with only the Direct and Raman terms; the poorness of the fit indicates that the Orbach term is required.

To calculate the exchange coupling, J, we assume that the spin state for each iron site in **3a** is $S_3 = 3/2$ (Fe^{III}) and $S_4 = 1$ (Fe^{IV}), which was established by the Mössbauer data in Figure 5. The splitting Δ between the S = 1/2 and S = 3/2 spin manifolds is $\Delta = -3J$ ($-2JS_1 \bullet S_2$), which gives J = –30±10 cm^{-1}.

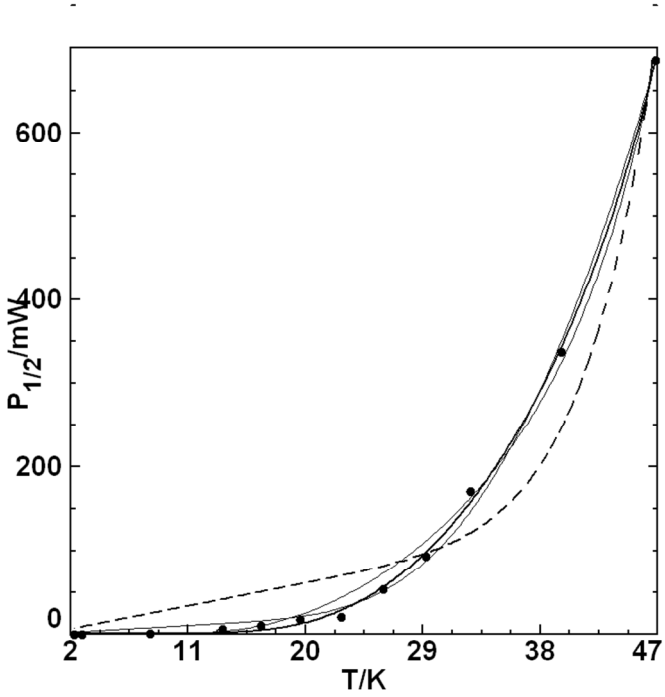

Figure S5. A plot of $P_{½}$ vs. T for the power saturation of **3a**. The fit to eq S1 (solid line) uses A = 5.7×10^{-2} mW/K, B = 1.771×10^{-13} mW/K, C = 7.2×10^{3} mW, Δ = 126 K. The two thin lines are for Δ = 180 K and 70 K. The dashed line is a fit without the Orbach relaxation term.

Alternate Formation of 3a

The formation of complex **3a** from **2a** was examined. Complex **2a** was dissolved in CH_3CN and an amount of this solution was added to the phosphate buffer (pH 11.8) containing 50% glycerol to give a solution with 20% CH_3CN. This mixture was transferred to an EPR tube and frozen. The EPR spectrum of this sample in the g = 2 region is identical to that of **3a** in Figure 3. No other EPR signals were present. Quantitation of the signal indicated 20% of the total Fe in the sample was **3a**. This is consistent with previous studies at pH 11.7 showing that **2a** converts to a mixture of predominately complexes $Fe^{IV}Fe^{IV}$ and $Fe^{IV}O$.[2,4]

The reduction of **2a** was also attempted with decamethylferrocene, $[Fe(Cp^*)_2]$. An EPR sample was prepared by addition of 4 eq of $[Fe(Cp^*)_2]$ to a solution of **2a** in CH_3CN. The EPR spectrum of this sample displays two signals: the S = ½ signal of **3a**, and the S = 3/2 signal of **1a**. The quantitation of the signals indicated that 35% and 20% of the Fe was converted to **3a** and **1a**, respectively. While we cannot presently account for the remaining Fe, this experiment demonstrates that **3a** can be produced from **2a** in the presence of a reductant.

The formation of **3a** from $Fe^{IV}O$ was attempted at pH 13. First, $Fe^{IV}O$ was prepared as previously reported, with the addition of 0.5 eq of *t*-BuOOH to **1a** at pH 13.[4] This sample produced an electronic absorption spectrum identical to that of $Fe^{IV}O$. To this solution, 1 eq of **1a** was added. The resulting absorption spectrum was composed of a sum of the spectra of complexes **1a** and $Fe^{IV}O$. In particular, the absorption from **3a** at 760 nm was not present. The spectrum did not change over the course of 1 h, indicating that there is no reaction between **1a** and $Fe^{IV}O$ at pH 13.

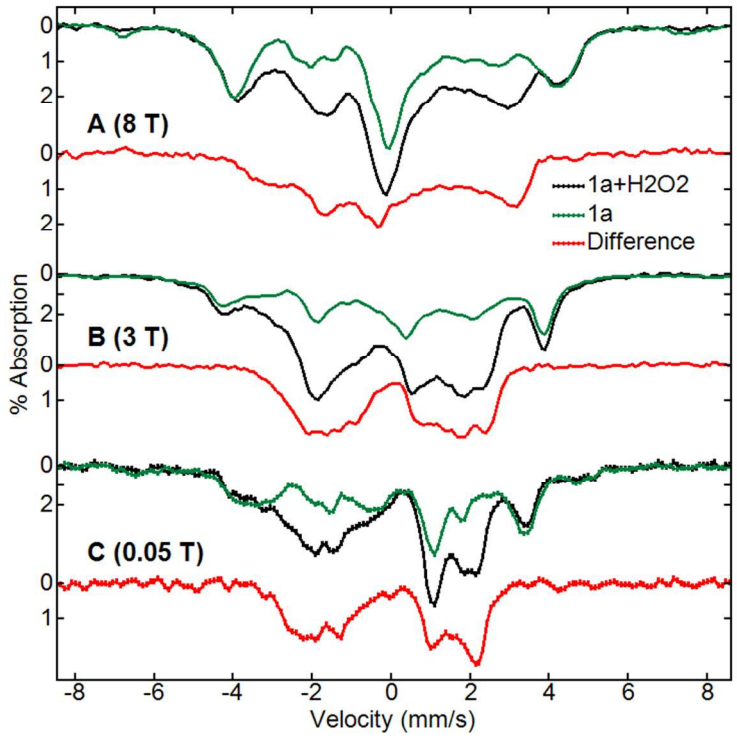

Figure S6. Mössbauer spectra of **1a** (black lines), **1a** + 1 eq. H_2O_2, and **3a** (difference, red lines) in pH 11.8 buffer, 50% glycerol, recorded at 4.2 K with an applied field of 8 T (A), 3 T (B) and 0.05 T (C). The difference spectra (also shown in Figure 6) are after subtraction of 45% of the area the corresponding spectra of **1a**.

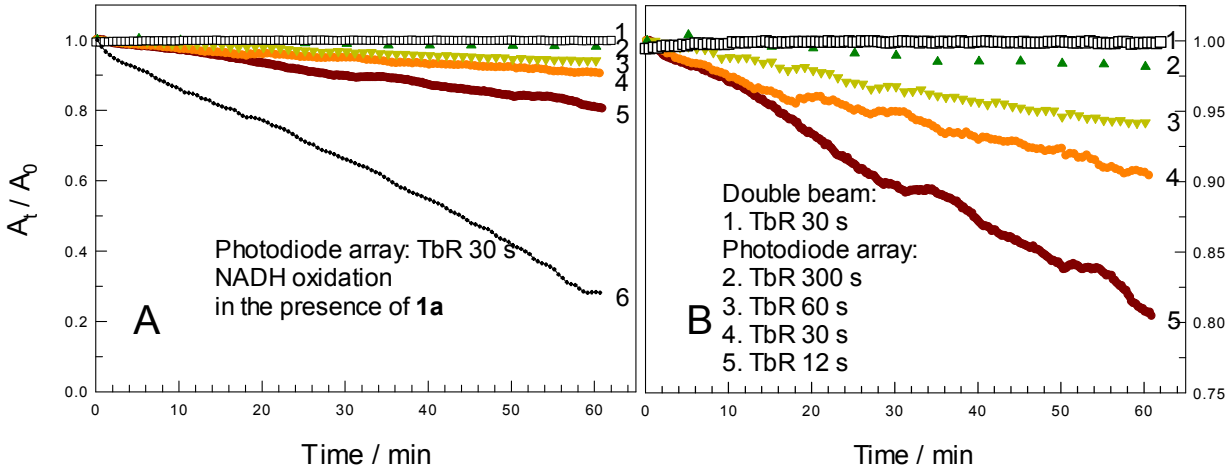

Figure S7. A. Kinetic curves for NADH oxidation in both the absence and presence of **1a** registered with both double beam (Curve 1) and photodiode array instrument (Curves 2-6) applying different pulse frequencies for the latter instrument. An NADH degradation curve (6) in the presence of **1a** was shown for comparison in S7A. **B**. Y axis zoom for the five runs of **A** in which **1a** was absent (Curves 1-5). TbR is the time between recording successive spectra. Other conditions: pH 10, w_0 10, [NADH] 5.14×10^{-5} M.

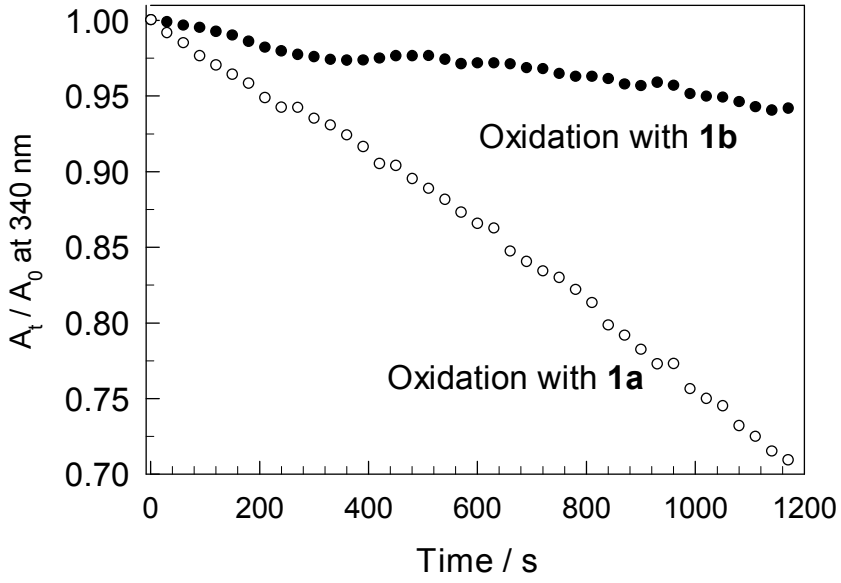

Figure S8. Changes of absorbance of NADH at 340 nm during **1a-** and **1b-**catalyzed oxidation of NADH by O_2 at pH 10 and w_0 3. Conditions: **1a**-catlayzed NADH oxidation: [NADH] 5.16×10^{-5} M, [**1a**] 2.47×10^{-6} M; **1b**-catlayzed NADH oxidation: [NADH] 5.16×10^{-5} M, [**1b**] 2.45×10^{-6} M.

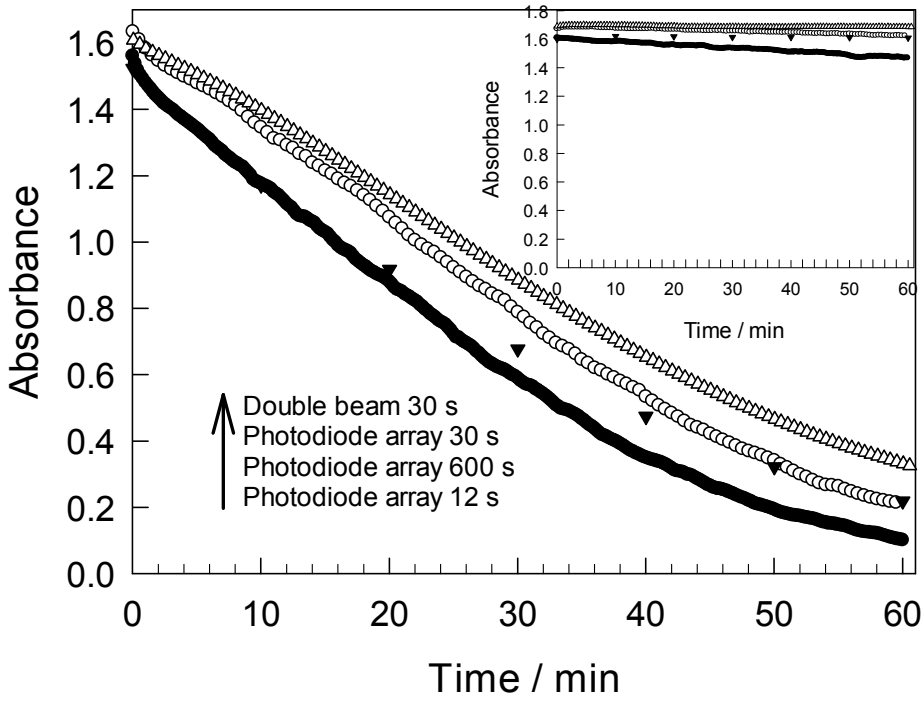

Figure S9. Catalyzed Pinacyanol chloride (PNC) oxidation by **1a** applying different pulse frequencies using photodiode array and double beam spectrometer. Conditions: pH 10, w_0 10, [PNC] = 2.71×10^{-5} M, [**1a**] = 1.52×10^{-6} M. Inset: PNC oxidation in the absence of **1a**. Time between recordings of successive spectra is 12, 30 and 600 s.

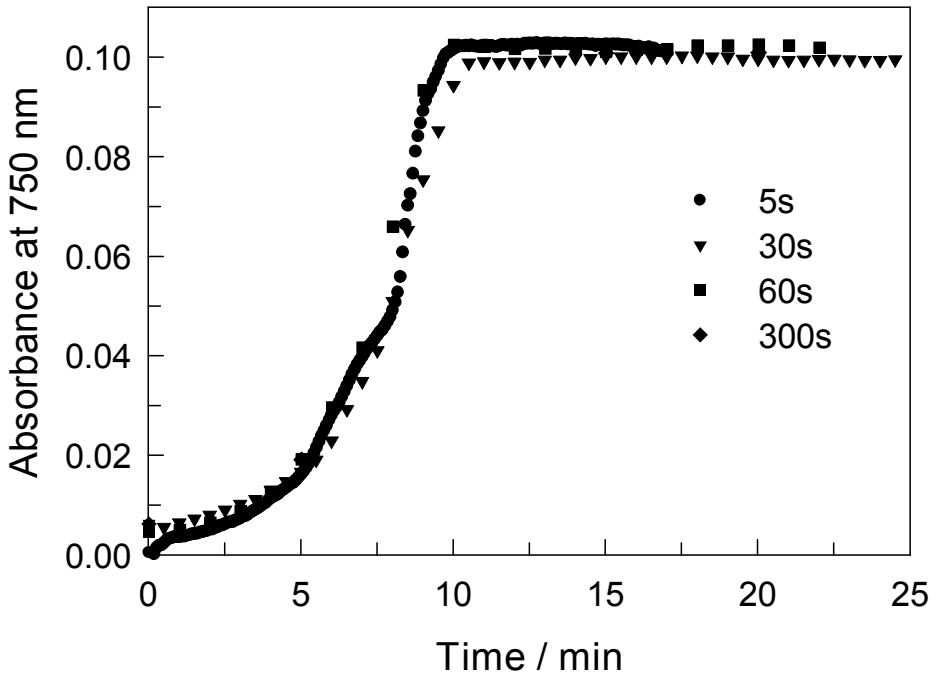

Figure S10. Absorbance change of **1a** at 750 nm applying different TbR (time between recordings of successive spectra) in the reverse micelles. Conditions: pH 12, w_0 15, [**1a**] = 1.36×10^{-4} M. Spectra were recorded every 5 s, 30 s, 60 s and 300 s using photodiode array UV-vis.

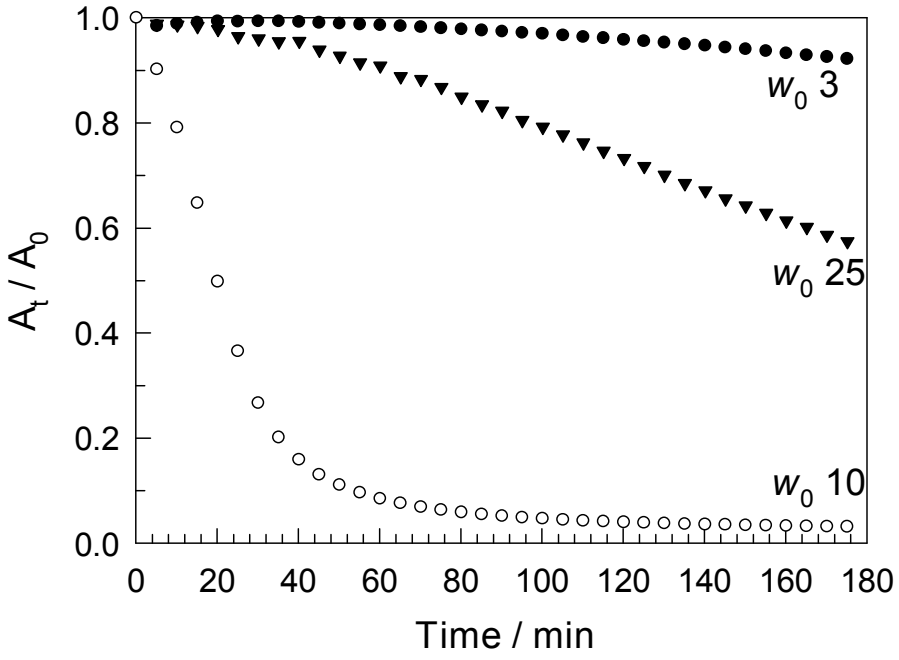

Figure S11. Changes of percentage of PNC during **1a**-catalyzed bleaching of PNC by O_2 at pH 10 and variable w_0 (3, 10 and 25) calculated by absorbance of PNC at 600 nm. Conditions: [PNC] 4.5×10^{-5} M, [**1a**] 5.0×10^{-6} M.

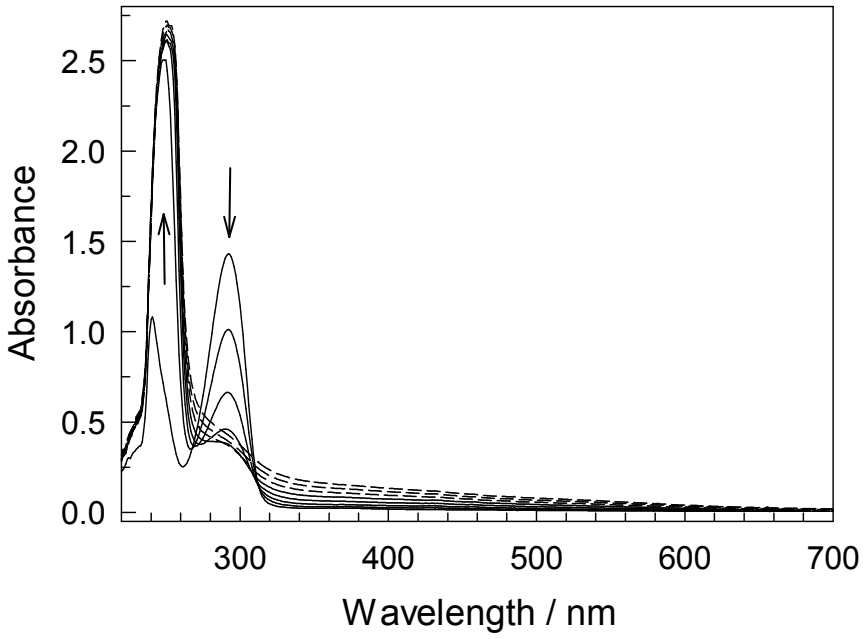

Figure S12. Spectral changes that accompany **1a-**catalyzed oxidation of hydroquinone by O_2. Conditions: [HQ] 6.0×10^{-4} M, [**1a**] 2.5×10^{-6} M, w_0 10, pH 10, spectra were recorded every 100 min. Solid and dash lines show the primary and secondary oxidative processes, respectively.

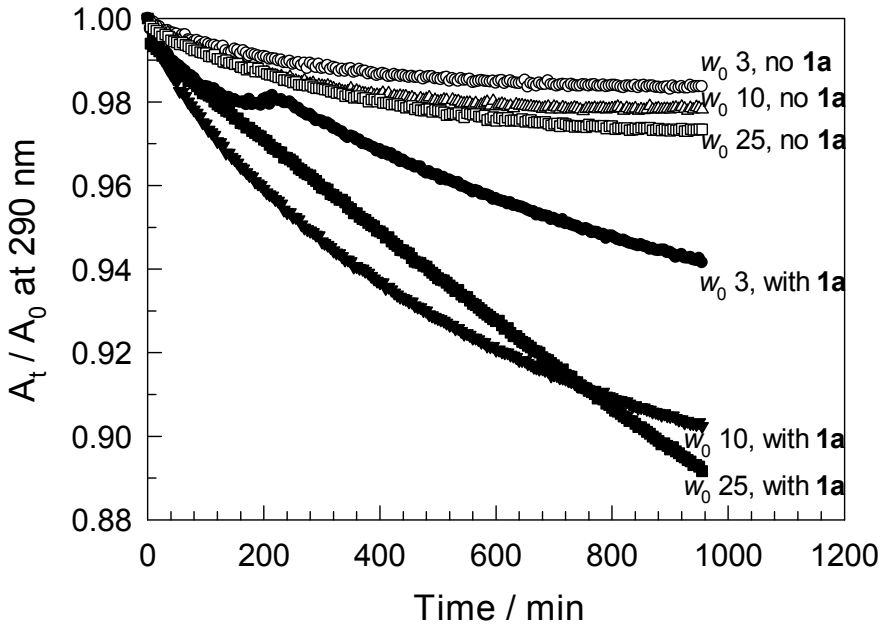

Figure S13. Hydroquinone oxidation under different conditions. Conditions: pH 8, [HQ] 6.0×10^{-4} M, [**1a**] 2.5×10^{-6} M, w_0 3, 10, 25.

References

(1) Markham, K. A.; Kohen, A. *Curr. Anal. Chem.* **2006**, *2*, 379-388.

(2) Ghosh, A.; Tiago de Oliveria, F.; Toshihiro Yano, T.; Nishioka, T.; Beach, E. S.; Kinoshita, I.; Münck, E.; Ryabov, A. D.; Horwits, C. P.; Collins, T. J. *J. Am. Chem. Soc.* **2005**, *127*, 2505-2513.

(3) Abragam, A.; Bleaney, B. *Electron Paramagnetic Resonance of Transition Ions (International Series of Monographs on Physics)*; Oxford Univ. Press: New York, 1970.

(4) Chanda, A.; Shan, X.; Chakrabarti, M.; Ellis, W.; Popescu, D.; Tiago de Oliveria, F.; Wang, D.; Que, L., Jr.; Collins, T. J.; Münck, E.; Bominaar, E. L. *Inorg. Chem.* **2008**, *47*, 3669-3678.